Acta Crystallographica Section D
Biological Crystallography
ISSN 0907-4449

Structure of the C subunit of V-type ATPase from *Thermus thermophilus* at 1.85 Å resolution

Nobutaka Numoto,[a] Akiko Kita[a] and Kunio Miki[a,b]*

[a]Department of Chemistry, Graduate School of Science, Kyoto University, Sakyo-ku, Kyoto 606-8502, Japan, and [b]RIKEN Harima Institute/SPring-8, Koto 1-1-1, Mikazuki-cho, Sayo-gun, Hyogo 679-5148, Japan

Correspondence e-mail: miki@kuchem.kyoto-u.ac.jp

Received 5 January 2004
Accepted 9 February 2004

PDB Reference: C subunit of V_0V_1-ATPase, 1v9m.

The V-type H^+-ATPases are similar to the F-type ATP synthases in their structure and functional mechanism. They hydrolyze ATP coupled with proton translocation across a membrane, but in some archaea and eubacteria they also synthesize ATP in the reverse reaction. The C subunit is one of the components of the membrane-bound V_0 moiety of V-type ATPases. The C subunit of V-type H^+-ATPase from *Thermus thermophilus* was crystallized in a monoclinic form and its crystal structure was determined at 1.85 Å resolution by the MAD method using selenomethionyl protein. The structure has a cone (tapered cylinder) shape consisting of only two types of helix (long and short) as secondary-structure elements. The molecule is divided into three similar domains, each of which has essentially the same topology. On the basis of the structural features and molecular-surface charge distribution, it is suggested that the bottom side of the C subunit is a possible binding site for the V_0 proteolipid L-subunit ring and that the C subunit might function as a spacer unit between the proteolipid L-subunit ring and the rotating V_1 central shaft.

1. Introduction

V-type H^+-ATPases (V_0V_1-ATPases), which are classified into the ATPase/ATP synthase superfamily, couple an ATP-hydrolysis/synthesis reaction with proton translocation across a membrane. In eukaryotic cells, V_0V_1-ATPases are present in the membranes of intracellular compartments, such as lysosomes, endosomes and clathrin-coated vesicles, and in plasma membranes (Nishi & Forgac, 2002). Their functions are widespread, including the acidification of intracellular compartments, renal acidification, bone resorption and tumour metastasis. In prokaryotic cells, V_0V_1-ATPases are found in the plasma membranes of some archaea and eubacteria. These prokaryotic V_0V_1-ATPases synthesize ATP coupled with proton flux across the plasma membranes (Yokoyama *et al.*, 1998). V_0V_1-ATPase, similar to F-type ATP synthase (F_0F_1-ATPases) which synthesizes ATP in mitochondria, chloroplasts and plasma membranes of eubacteria (Yoshida *et al.*, 2001), consists of two functional sets of subunits: a peripheral V_1 or F_1 moiety responsible for ATP hydrolysis/synthesis and a membrane-integrated V_0 or F_0 moiety responsible for proton translocation. Both V_0V_1-ATPases and F_0F_1-ATPases have a similar rotary mechanism of function (Imamura *et al.*, 2003; Yokoyama, Nakano *et al.*, 2003).

The V_0V_1-ATPase from the thermophilic eubacterium *Thermus thermophilus* is composed of nine subunits, A, B, D, F, C, E, G, I and L, with molecular weights of 64, 54, 25, 12, 36, 21, 13, 72 and 8 kDa, respectively (Yokoyama,

Nagata *et al.*, 2003). The V_1 moiety consists of four subunits, with stoichiometry $A_3B_3D_1F_1$. The A subunit, which is a counterpart of the catalytic β subunit of F_0F_1-ATPase, forms an alternating A_3B_3 hexamer ring with the B subunit that surrounds a central shaft composed of D and F subunits. The V_0 moiety contains the C, E, G, I and L subunits, of which the C, E and G subunits are hydrophilic. The L subunit forms a proteolipid ring with two transmembrane helices (Yokoyama *et al.*, 2000). The E, G and I subunits form a stator part. The C subunit, which is the counterpart of the d subunit of the eukaryotic V_0V_1-ATPase, is tightly bound to the L-subunit ring (Zhang *et al.*, 1992). It has been suggested that the C subunit is located on the cytoplasmic side of the membrane, making up part of the central shaft (Adachi *et al.*, 1990; Chaban *et al.*, 2002). There is no corresponding part in F-type ATP synthase.

The crystal structure of subunit H of V_0V_1-ATPase from *Saccharomyces cerevisiae* has been reported (Sagermann *et al.*, 2001) and is the only known V_0V_1-ATPase structure at atomic resolution; this subunit has no counterpart in *T. thermophilus* V_0V_1-ATPase. We have determined the structure of a monoclinic $P2_1$ crystal of the C subunit of V_0V_1-ATPase from *T. thermophilus* at 1.85 Å resolution. The structure of the C subunit of V_0V_1-ATPase from the same species was determined very recently from a different crystal form (hexagonal $P6_1$) at 1.95 Å resolution and was published just prior to the submission of this report (Iwata *et al.*, 2004). The structures from the two crystal forms appear to be essentially the same, supporting the idea that the C subunit is located on the L-subunit ring in the central part of the V_0 moiety of V-type ATPase.

2. Materials and methods

2.1. Expression and purification

N-terminal (residues 1–150) and C-terminal (residues 151–969) fragments of the gene for the C subunit were amplified by PCR. The primers for the N-terminal fragment, which contained artificial *Nde*I and *Afl*II sites (in bold), were 5′-ATAT**CATATG**GCTGACGACTTCGCCTACCT-3′ and 5′-ACCGCC**CTTAAG**GCGCGGGCCAAGGGGTGG-3′. The primers for the C-terminal fragment, which contained artificial *Afl*II and *Bam*HI sites (in bold), were 5′-CGCGC**CTTAAG**GGCGGTCCTGCGGGAGACG-3′ and 5′-ATAT**GGATCC**TTATTACGGGCACACCACCTCCTCCTCCACCT-3′. The PCR products were digested with *Nde*I, *Afl*II and *Bam*HI and were ligated into pET11a expression plasmid (Novagen), in which the C-subunit gene is under the control of the T7 promoter. This recombinant plasmid was transformed into *Escherichia coli* strain BL21 (DE3). Cells were grown at 310 K in Luria–Bertani medium containing 50 µg ml^{-1} ampicillin and were harvested and sonicated in 20 m*M* Tris–HCl buffer pH 8.0 containing 50 m*M* NaCl and 2-mercaptoethanol. The crude extract was incubated at 343 K for 10 min, cooled on ice and ultracentrifuged at 200 000*g* for 60 min. Ammonium sulfate was added to the supernatant to a final concentration of 1.2 *M* and the solution was loaded onto a Resource PHE column (Amersham Bioscience) equilibrated with 50 m*M* sodium phosphate buffer pH 7.0 containing 1.2 *M* ammonium sulfate and eluted with a linear gradient of ammonium sulfate. The fractions containing the C subunit were applied onto a Resource Q column (Amersham Bioscience) equilibrated with 50 m*M* Tris–HCl buffer pH 9.0 and eluted with a linear gradient of NaCl. The fractions containing the C subunit were applied onto a hydroxyapatite CHT10 (Bio-Rad) column equilibrated with 10 m*M* sodium phosphate buffer pH 7.0 and eluted with a linear gradient of sodium phosphate. The fractions containing the C subunit were applied onto a HiLoad 16/60 Superdex 75 (Amersham Bioscience) column equilibrated with 20 m*M* Tris–HCl buffer pH 8.0 containing 150 m*M* NaCl. The fractions containing subunit C were concentrated to 28 mg ml^{-1} using an ultrafiltration membrane in solutions of 20 m*M* Tris–HCl buffer pH 8.0 containing 150 m*M* NaCl and 1 m*M* dithiothreitol and stored at 277 K.

In the case of the selenomethionine-labelled C subunit, cells were grown at 310 K in LeMaster medium (LeMaster & Richards, 1985) supplemented with 50 µg ml^{-1} selenomethionine, 1.0%(*w*/*v*) lactose, 50 µg ml^{-1} ampicillin and vitamin mixture (Kao and Michayluk Vitamin Solution, Sigma) in place of methionine and glucose. Protein expression was induced without IPTG in *E. coli* B834 (DE3) for 24 h. The subsequent steps were the same as described above except that the protein concentration was 18 mg ml^{-1}.

2.2. Crystallization

Both native and selenomethionine-labelled C-subunit proteins were crystallized from essentially the same conditions using the sitting-drop vapour-diffusion method at 293 K. Reservoir solution containing 0.1 *M* Tris–HCl pH 8.5, 20–28%(*v*/*v*) PEG 300, 5%(*v*/*v*) PEG 8000 and 10%(*v*/*v*) glycerol was mixed with protein solution in a 1:1 ratio. Crystals appeared after one week.

2.3. Data collection and structure determination

X-ray diffraction data were collected on the BL45XU beamline at SPring-8 using a Rigaku R-AXIS V imaging-plate detector. The crystals were flash-frozen in a nitrogen-gas stream at 90 K. Crystals of the native and selenomethionyl proteins diffracted X-rays to 1.85 and to 2.1 Å resolution, respectively. Both crystals belong to space group $P2_1$, with unit-cell parameters $a = 41.79$, $b = 83.81$, $c = 48.57$ Å, $\beta = 113.86^\circ$ for the native crystals and $a = 42.02$, $b = 84.00$, $c = 48.73$ Å, $\beta = 114.03^\circ$ for the selenomethionyl crystals. The asymmetric unit of both crystals contains one molecule of the C subunit, with Matthews coefficients of 2.17 and 2.19 Å^3 Da^{-1}, respectively (Matthews, 1968). A complete data set was collected from a single crystal, changing the exposure points at each wavelength. The diffraction data were processed with the *HKL*2000 package (Otwinowski & Minor, 1997). The MAD method was employed for structure determination using crystals of the selenomethionine-labelled C subunit. Local scaling, determination of the Se-atom positions and initial

Table 1
Data-collection and refinement statistics for the C subunit.

Values in parentheses are for the highest resolution shell.

Data set	Native	Edge	Peak	Remote
Wavelength (Å)	1.0000	0.9795	0.9793	0.9781
Space group	$P2_1$			
Unit-cell parameters				
a (Å)	41.79	42.02		
b (Å)	83.81	84.00		
c (Å)	48.57	48.73		
β (°)	113.86	114.03		
Resolution (Å)	50.0–1.85 (1.92–1.85)	50.0–2.10 (2.18–2.10)		
No. of reflections				
Measured	91048	132658	133440	133719
Unique	25341	17663	17724	17698
Completeness (%)	97.1 (91.5)	97.8 (94.0)	98.1 (94.5)	97.6 (93.5)
$R_{\rm merge}$† (%)	6.1 (33.8)	5.1 (8.9)	5.5 (8.3)	5.3 (11.3)
Multiplicity	3.5	7.5	7.5	7.6
Phasing statistics				
Resolution		50.0–2.10		
Mean figure of merit (overall/centric/acentric)		0.73/0.62/0.73		
Refinement statistics				
Resolution	20–1.85			
σ cutoff	0.0			
$R_{\rm work}$ (%)	20.2			
$R_{\rm free}$ (%)	22.8			
No. of atoms				
Protein	2458			
Water	165			
Glycerol	12			
R.m.s. deviations				
Bond length (Å)	0.005			
Bond angles (%)	1.0			
Ramachandran plot				
Most favourable (%)	95.6			
Additional allowed (%)	4.4			

† $R_{\rm merge} = \sum\sum_i |I(h) - I(h)_i| / \sum\sum_i I(h)$, where $I(h)$ is the mean intensity after rejections.

phase calculation were performed with *SOLVE* (Terwilliger & Berendzen, 1999) followed by density modification with *RESOLVE* (Terwilliger, 2000). Two Se positions of the three expected in the asymmetric unit were successfully determined and a clearly interpretable electron-density map was obtained with an overall figure of merit of 0.73. An initial model consisting of 309 out of 323 residues (96%) was built with *ARP/wARP* (Perrakis *et al.*, 1999) using the 1.85 Å native data and the obtained MAD phases. Several cycles of manual model rebuilding and model refinement were performed using *O* (Jones *et al.*, 1991) and *CNS* (Brünger *et al.*, 1998), respectively. For further refinement, 5% of the reflections were set apart as a random test set for the calculation of $R_{\rm free}$ values. After each cycle, $2F_{\rm o} - F_{\rm c}$ and $F_{\rm o} - F_{\rm c}$ electron-density maps were calculated to check the fit of the model to the map. Water molecules were picked up from the $F_{\rm o} - F_{\rm c}$ map on the basis of peak heights and distance criteria. A total of 165 water molecules and two glycerol molecules were included in the final model, which had R and $R_{\rm free}$ values of 20.2 and 22.8%, respectively. Evaluation of the quality of the model was performed with *PROCHECK* (Laskowski *et al.*, 1998; Collaborative Computational Project, Number 4, 1994) and 95.6% of the residues were found to be in the most favoured regions of the Ramachandran plot; 4.4% of residues lie in additional allowed regions. The data-collection and refinement statistics are summarized in Table 1.

3. Results and discussion

The overall structure of the C subunit is highly helix-rich, containing helices H1–H20 (Fig. 1). The molecule is apparently composed of three domains (Fig. 2). The overall structure and topology diagram of the C subunit determined using the monoclinic crystal is essentially the same as that determined using hexagonal crystals (Iwata *et al.*, 2004). Domain I consists of N-terminal residues 5–77 and C-terminal residues 282–323. Domains II and III consist of residues 78–178 and residues 186–281, respectively; residues 1–4 and 179–185 are disordered. Each of the three domains, which have highly similar folds and the same topology, is essentially composed of two relatively long helices of 40–50 Å in length and four shorter helices (except for H1 and H6 of domain I). The six longer helices (H5, H7, H12, H13, H18 and H19) form a central cavity that is accessible from one side. The other 12 helices, including five 3_{10}-helices (H4, H8, H14, H16 and H17), are located around six central long helices that constitute the rim. Two helices of domain I, H1 and H6, are topologically disordered, but H6 can be interpreted as part of the long helix H5. All the helices run roughly in parallel, forming a cone (tapered cylinder) shape with a height of 45 Å and an approximate diameter of 50 Å at the top and 20 Å at the bottom. This is not

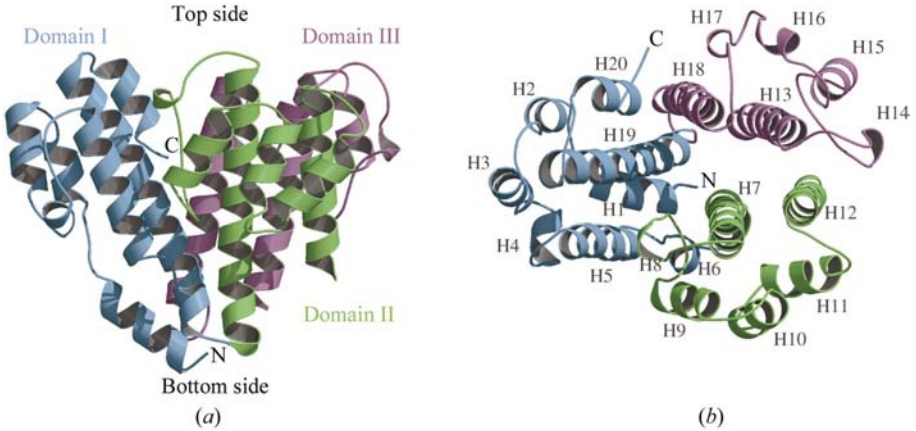

Figure 1
A ribbon model of the overall structure of the C subunit of V_0V_1-ATPase from *T. thermophilus*. Domains I, II and III are shown in cyan, green and magenta, respectively. The N- and C-termini are labelled N and C, respectively. (*a*) Side view. The top and bottom sides referred in the text are indicated. (*b*) View from the top side. The 20 helices are labelled H1–H20. These figures were prepared using the programs *MOLSCRIPT* (Kraulis, 1991) and *RASTER3D* (Merritt & Bacon, 1997).

long enough to pass through the membrane, supporting the previous reports that the C subunit is not a transmembrane subunit but is placed on the cytoplasmic side (Adachi *et al.*, 1990; Chaban *et al.*, 2002). A sequence alignment of the C subunit with those from other species shows that Glu296 is highly conserved among the various species (Fig. 3). This residue is located in the central long helix H19 and is hydrogen-bonded to the main-chain amino group of Leu20 (also a conserved residue) placed in a loop region connecting H1 and H2, contributing the connection between the C- and N-terminals to form domain I (Fig. 4). A comparison of the three domains shows H1 of domain I to be an insertion helix; there is no corresponding part in the other two domains. The side chain of Glu296 has an appropriate length and flexibility to reach the main chain of loop H1–H2, suggesting that Glu296 might be essential to maintain the overall fold of the C subunit. In addition, another conserved residue, Tyr45 (H4), is also located in this region, forming a hydrophobic core that stabilizes the central helices and the surrounding rim helices. Cys267 and Cys322 form a disulfide bond in the present crystal structure, but both residues are not conserved; therefore, this could be less important in maintaining fold or function.

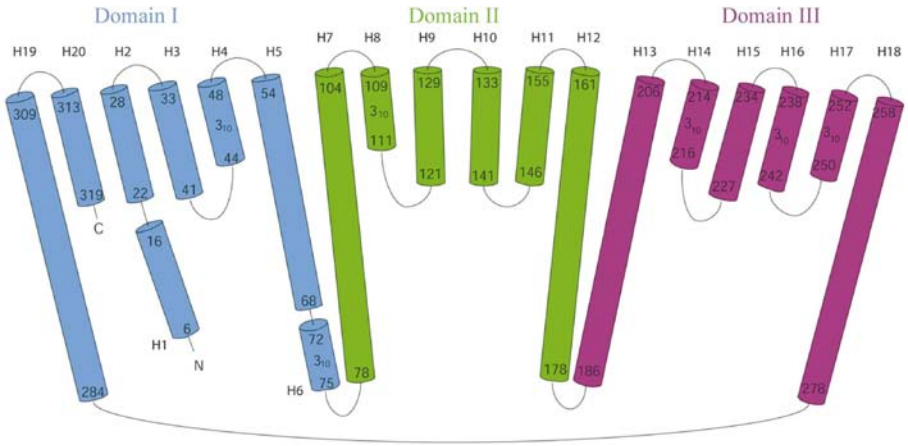

Figure 2
Topology diagram of the C subunit from *T. thermophilus*. The cylinders represent α-helices; 3_{10}-helices are labelled 3_{10}. The colours of the three domains are the same as in Fig. 1. The slightly tilted arrangement of the cylinders corresponds to the cone-shaped helix assembly in the three-dimensional structure. All domains are composed of six long helices and four short helices with the same topology, except for H1 and H6 which are additional components of domain I. Domain I consists of the N-terminal H1–H6 and the C-terminal H19–H20. The numbers in each cylinder refer to the residues located at the N- and C-termini of each helix.

The C subunit of the V_0 part of V_0V_1-ATPases is suggested to interact with the V_0 proteolipid L subunits, which are thought to form a ring structure spanning the membrane. There is no structural information on the L-subunit ring and still no definite information on how many L subunits form such a proteolipid ring. Sequence alignment between the c subunit of the *E. coli* F_0 part and the L subunit from *T. thermophilus* indicated a significant similarity (Yokoyama *et al.*, 2000) and the NMR structure of the *E. coli* c subunit has been determined (Rastogi & Girvin,

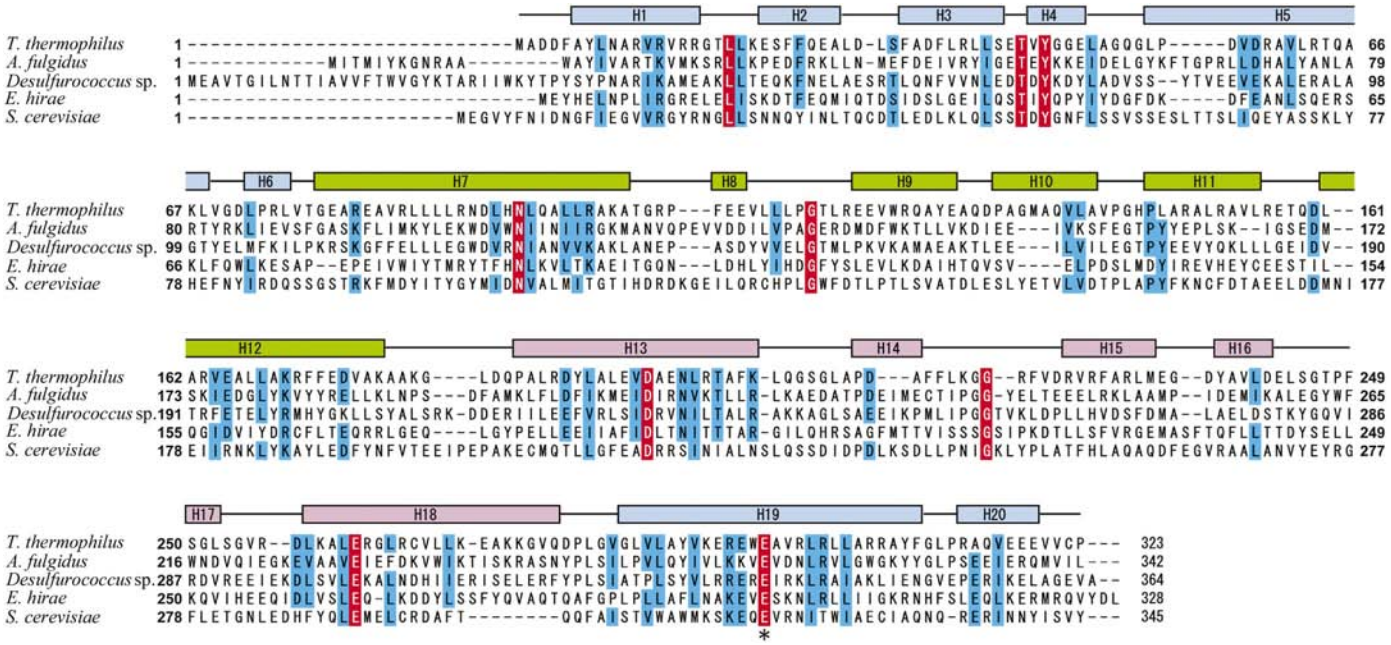

Figure 3
Comparison of the amino-acid sequences of the C subunit from *T. thermophilus*, *Archaeoglobus fulgidus* (archaea), *Desulfurococcus* sp. (archaea), *Enterococcus hirae* (bacteria) and *S. cerevisiae* (eukarya) with the secondary structure from the three-dimensional structure of the C subunit from *T. thermophilus*. Identical and relatively conserved residues are highlighted in red and blue, respectively. The secondary structures are shown in boxes above the sequence and the position of the conserved Glu296 is indicated with an asterisk.

1999; PDB code 1c17). In this structure, there is a cavity with a diameter of 30 Å at the centre of the transmembrane ring composed of 12 c subunits. Because of the sequence similarity, it is expected that a similar V_0 proteolipid ring is also constructed in V_0V_1-ATPases and consists of 12 L subunits as found in the structure of the *E. coli* c subunit. In the C subunit of *T. thermophilus*, the bottom region, which is mainly composed of the lower parts of the central six long helices, has a diameter of about 30 Å at the boundary between the top region and the bottom region. This diameter is comparable with that of the expected central cavity of the L-subunit ring, suggesting that the bottom region of the C subunit is suitable in size for binding to the central cavity of the L-subunit ring in the V_0 part of V_0V_1-ATPases (Iwata *et al.*, 2004). Furthermore, this hypothesis is supported by the electrostatic features of the molecular surface. The molecular surface of the C subunit is generally charged (Fig. 5). On the top side, the region around the entrance of the central cavity is almost hydrophobic. On the other hand, the bottom side is essentially charged. In particular, in the boundary region between the top and bottom regions (around the white circle in Fig. 5*a*) there is a positively charged ring region with an approximate diameter of 30 Å that is mainly contributed by positively charged residues such as Lys67, Lys178 and Lys275. The hydropathy profile of the L subunit indicates a cytoplasmic loop region of two transmembrane helices; the conserved residue Glu66 is located in this loop region (Yokoyama *et al.*, 2000). When the L subunit is compared with the structure of the *E. coli* c-subunit ring (Rastogi & Girvin, 1999), Glu66 is expected to be located at the inner edge of the cavity of the L-subunit ring. Glu66 of each L subunit is expected to take part in a negatively charged ring around the edge of the entrance of the cavity of the L-subunit ring. The positively charged part of the bottom side of the C subunit might be suitable for the binding site with the V_0 proteolipid ring.

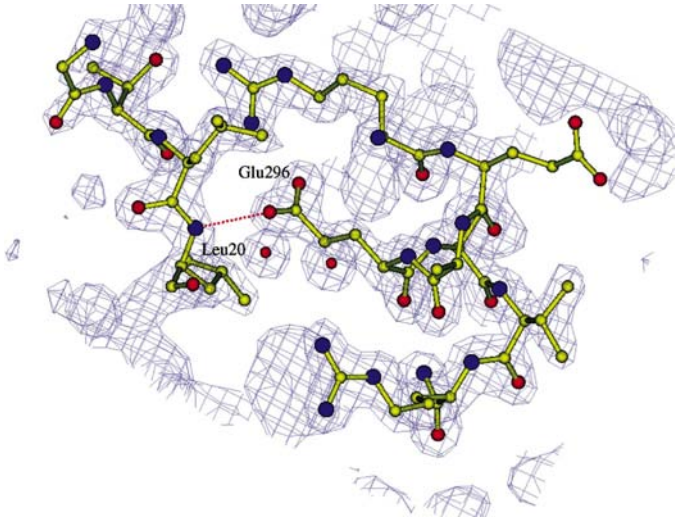

Figure 4
The σ_A-weighted $2F_o - F_c$ electron-density map (>1.5σ) with a superimposed ball-and-stick model of the final structure in the region containing the conserved residue Glu296. The side chain of Glu296 (H19) interacts with the main chain of Leu20 (the loop region H1–H2) with a hydrogen-bond distance of 2.71 Å. Figures were prepared with the programs *MOLSCRIPT* (Kraulis, 1991) and *CONSCRIPT* (Lawrence & Bourke, 2000).

The *B* values of the loop regions are informative. The loop regions are classified into three categories. The loops on the top side (loops H19–H20, H2–H3, H4–H5, H7–H8, H9–H10, H11–H12, H13–H14, H15–H16 and H17–H18) and on the bottom side (loops H6–H7, H12–H13 and H18–H19) have higher *B* values; the average *B* values of atoms in the loop regions on the top and bottom sides are 25.4 and >35.3 Å^2, respectively, although the atoms of the loop H12–H13 on the bottom side are highly disordered and could not be located. In contrast, the loops of the short helices in the boundary between the top and bottom regions (loops H3–H4, H8–H9, H10–H11, H14–H15 and H16–H17) have relatively small *B* values (average *B* values of 21.3 Å^2).

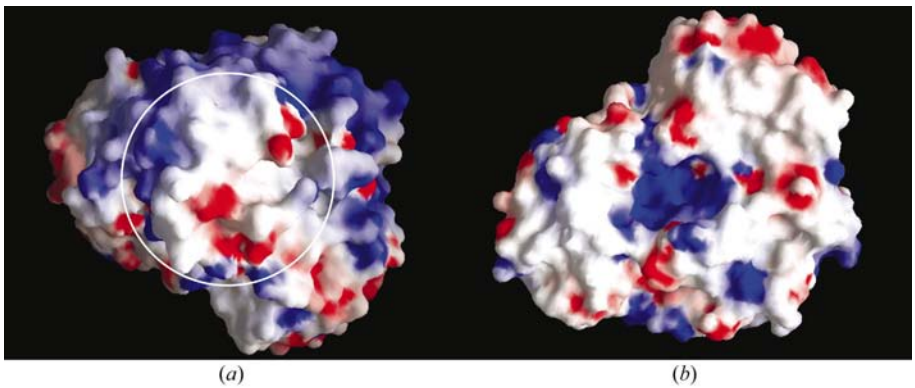

Figure 5
Charge distribution of the molecular surface of the C subunit. Negatively and positively charged surfaces are coloured red and blue, respectively. (*a*) The bottom surface area as viewed from the opposite viewpoint to that in Fig. 1(*b*). The white circle indicates the boundary between the top and bottom regions. The diameter of the circle is about 30 Å. The positively charged region spreads out of the circle indicating the binding site for the L-subunit ring, which is expected to have a negatively charged ring region (see text). (*b*) The top surface area as viewed from the same viewpoint as Fig. 1(*b*). The figures were calculated and represented using the program *GRASP* (Nicholls *et al.*, 1991).

It is expected that the loops on the bottom side contact the L-subunit ring as mentioned above and the surface loops on the top side interact with the D and F subunits which compose the central shaft of the V_1-ATPase (Imamura *et al.*, 2003). The function of the central cavity of the C subunit is still unclear. Since Glu294 located in the inner cavity is conserved, this residue could participate in the interaction with the central shaft composed of D and F subunits.

V_0V_1-ATPases and F_0F_1-ATPases have similar structures and common functional mechanisms (Imamura *et al.*, 2003; Yokoyama, Nakano *et al.*, 2003), but the C subunit is characteristic of V-type ATPases. It is suggested that the C subunit functions as a spacer unit in the proteolipid L-subunit ring that

plays a role in proton translocation and rotating the V_1 central shaft. The tight binding of the C subunit to the L-subunit ring (Zhang *et al.*, 1992) may be necessary to transmit the torque to the V_1 central shaft for ATP synthesis.

We would like to thank Dr Y. Kawano and Mr Nakajima of SPring-8 for their help with the X-ray diffraction experiments. This work was performed under the Structurome Project of RIKEN Harima Institute; the protein-sample preparation carried out by Professor S. Kuramitsu and his coworkers is greatly appreciated. This work was supported by a grant of the National Project on Protein Structural and Functional Analyses from the Ministry of Education, Culture, Sports, Science and Technology of Japan.

References

Adachi, I., Puopolo, K., Marquez-Sterling, N., Arai, H. & Forgac, M. (1990). *J. Biol. Chem.* **265**, 967–973.
Brünger, A. T., Adams, P. D., Clore, G. M., DeLano, W. L., Gros, P., Grosse-Kunstleve, R. W., Jiang, J.-S., Kuszewski, J., Nilges, M., Pannu, N. S., Read, R. J., Rice, L. M., Simonson, T. & Warren, G. L. (1998). *Acta Cryst.* D**54**, 905–921.
Chaban, Y., Ubbink-Kok, T., Keegstra, W., Lolkema, J. S. & Boekema, E. J. (2002). *EMBO Rep.* **3**, 982–987.
Collaborative Computational Project, Number 4 (1994). *Acta Cryst.* D**50**, 760–763.
Imamura, H., Nakano, M., Noji, H., Muneyuki, E., Ohkuma, S., Yoshida, M. & Yokoyama, K. (2003). *Proc. Natl Acad. Sci. USA*, **100**, 2312–2315.
Iwata, M., Imamura, H., Stambouli, E., Ikeda, C., Tamakoshi, M., Nagata, K., Makyio, H., Hankamer, J. B., Yoshida, M., Yokoyama, K. & Iwata, S. (2004). *Proc. Natl Acad. Sci. USA*, **101**, 59–64.
Jones, T. A., Zou, J. Y., Cowan, S. W. & Kjeldgaard, M. (1991). *Acta Cryst.* A**47**, 110–119.
Kraulis, P. J. (1991). *J. Appl. Cryst.* **24**, 946–950.
Laskowski, R. A., Moss, D. S. & Thornton, J. M. (1998). *J. Mol. Biol.* **231**, 1049–1067.
Lawrence, M. C. & Bourke, P. (2000). *J. Appl. Cryst.* **33**, 990–991.
LeMaster, D. M. & Richards, F. M. (1985). *Biochemistry*, **24**, 7263–7268.
Matthews, B. W. (1968). *J. Mol. Biol.* **33**, 491–497.
Merritt, E. A. & Bacon, D. J. (1997). *Methods Enzymol.* **277**, 505–524.
Nicholls, A., Sharp, K. A. & Honig, B. (1991). *Proteins*, **11**, 281–296.
Nishi, T. & Forgac, M. (2002). *Nature Rev. Mol. Cell Biol.* **3**, 94–103.
Otwinowski, Z. & Minor, W. (1997). *Methods Enzymol.* **276**, 307–326.
Perrakis, A., Morris, R. & Lamzin, V. S. (1999). *Nature Struct. Biol.* **6**, 458–463.
Rastogi, V. K. & Girvin, M. E. (1999). *Nature (London)*, **402**, 263–268.
Sagermann, M., Stevens, T. H. & Matthews, B. W. (2001). *Proc. Natl Acad. Sci. USA*, **98**, 7134–7139.
Terwilliger, T. C. (2000). *Acta Cryst.* D**56**, 965–972.
Terwilliger, T. C. & Berendzen, J. (1999). *Acta Cryst.* D**55**, 849–861.
Yokoyama, K., Muneyuki, E., Amano, T., Mizutani, S., Yoshida, M., Ishida, M. & Ohkuma, S. (1998). *J. Biol. Chem.* **273**, 20504–20510.
Yokoyama, K., Nagata, K., Imamura, H., Ohkuma, S., Yoshida, M. & Tamakoshi, M. (2003). *J. Biol. Chem.* **278**, 42686–42691.
Yokoyama, K., Nakano, M., Imamura, H., Yoshida, M. & Tamakoshi, M. (2003). *J. Biol. Chem.* **278**, 24255–24258.
Yokoyama, K., Ohkuma, S., Taguchi, H., Yasunaga, T., Wakabayashi, T. & Yoshida, M. (2000). *J. Biol. Chem.* **275**, 13955–13961.
Yoshida, M., Muneyuki, E. & Hisabori, T. (2001). *Nature Rev. Mol. Cell Biol.* **2**, 669–677.
Zhang, J., Myers, M. & Forgac, M. (1992). *J. Biol. Chem.* **267**, 9773–9778.